

A novel synthesis of the N-13 labeled atmospheric trace gas peroxyntic acid

By T. Bartels-Rausch^{1,*}, Th. Ulrich^{1,2}, Th. Huthwelker¹ and M. Ammann¹

¹ Paul Scherrer Institut, Laboratory of Radiochemistry and Environmental Chemistry, 5232 Villigen PSI, Switzerland

² Universität Bern, Department of Chemistry and Biochemistry, 3008 Bern, Switzerland

(Received November 29, 2010; accepted in revised form January 14, 2011)

Synthesis / N-13 / Nitrogen oxides / Snow–air interface / Atmosphere / Cryosphere / PNA / HNO₄ / HO₂NO₂

Summary. Radioactively labeled trace gases have been successfully used to study heterogeneous chemistry of atmospheric relevance. Here we present a new synthesis of gas-phase peroxyntic acid labeled with ¹³N (H¹³NO₄) to study the interaction of HNO₄ with ice and snow surfaces. A yield of about 30% for HNO₄ was determined. The main by-products were HNO₃ and HNO₂. Exposure of an ice packed bed flow tube to these species revealed that the interaction with the surface scale in the order HNO₃ > HNO₄ = HNO₂ > NO₂.

1. Introduction

The interaction of atmospheric trace gases with the Earth's snow cover or ice surfaces is of high environmental relevance [1, 2]. The atmospheric trace gas that we focus on in this work is the nitrogen oxide peroxyntic acid (HNO₄). Nitrogen oxides have been of particular interest in atmospheric science, because their gas-phase concentration directly influences the ozone levels and the oxidative capacity of the atmosphere.

For example, in the lower atmosphere, HNO₃ adsorbs to and is thus scavenged by ice clouds [3]. Similarly, on the ground, trace gas uptake by snow may significantly alter the concentration both in the air above snow-covers and in the snow itself [4, 5]. Nitrous acid (HNO₂) partitions less to ice or snow, but its interactions with the ice are still strong enough to significantly slow down its diffusion through surface snow [6, 7]. This longer residence time in the snow pack, as compared to non-interacting species such as NO₂, makes its photolytic dissociation and thus its role as source of the strong oxidant OH more probable. Recently, Slusher *et al.* concluded that the uptake of HNO₄ by snow is of similar magnitude than observed for HNO₃ [8]. The finding that deposition to snow is a major loss process for gas-phase HNO₄ above Antarctic surface snow was based on steady-state calculations and comparison to field measurements. Taken its significant fraction of total nitrogen oxides in cold

regions of the atmosphere such as in Antarctica and the upper troposphere [9, 10], its uptake would significantly impact the budget of gas-phase nitrogen oxides. Also, as HNO₄ has a significant photo-dissociation cross section [11], its deposition should be taken into account when discussing the vivid photochemistry of nitrogen oxides in snow-packs [4]. Sound conclusions are however hampered by missing data from well-controlled laboratory experiments on the interaction of HNO₄ with ice or any other environmental surface.

¹³N with a half-life of 10 min has been used in the past to label nitrogen oxides to be used as tracer in chemical experiments with relevance to Earth's atmosphere [12]. The main aim of this work was to develop a new synthesis route for ¹³N labeled HNO₄ in the gas phase by an association reaction of ¹³NO₂ with HO₂. ¹³N isotopes are obtained from the PROTRAC facility at the Paul Scherrer Institute. In the first part of the work, we describe the yield of the product (HNO₄) and of other nitrogen oxide by-products by means of a chemical ionization mass spectrometer and of a chemiluminescence detector. This work was done with an excess of H¹⁴NO₄. As neither method can differentiate ¹³N from other nitrogen isotopes, the production of ¹³N labeled nitrogen oxides was verified using a packed bed flow tube for separation and radioactive decays for detection in a second step. This method has been called thermochromatography before [13]. In this work, ice was chosen as stationary phase, because the separation of HNO₃, HNO₂, NO₂, and of NO in an ice packed bed flow tube has been shown before [14] and additionally, first information on the partitioning of HNO₄ between ice and air can be gained.

2. Experimental

Fig. 1 shows a scheme of the experimental set-up consisting of the production of ¹³N in a gas target and of the synthesis of HNO₄ (Fig. 1a). Included is also a scheme of the packed bed flow tube that was used to verify the production of H¹³NO₄ (Fig. 1b) and of the analytical set-up to characterize the HNO₄ synthesis (Fig. 1c). The tubing of the flow system consisted of perfluoro-alkoxy copolymer (PFA) 4 mm i.d. Gas flows were controlled by mass flow controllers (Brooks Instruments) or by mass flow regulators (Vögtlin Instruments) both of which have a 1% full-scale accuracy.

* Author for correspondence
(E-mail: thorsten.bartels-rausch@psi.ch).

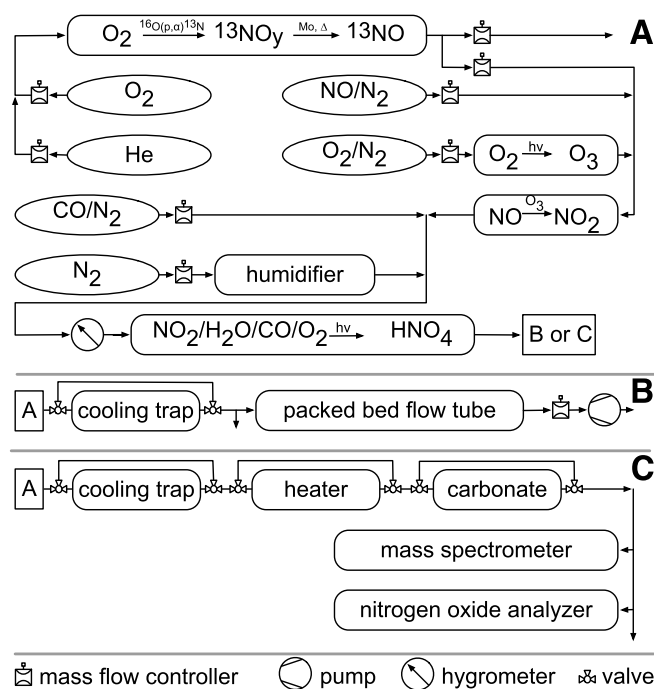


Fig. 1. Scheme of the experimental set-up. (a) shows the production of ^{13}N isotopes and the synthesis of HNO_4 molecules. The synthesis was coupled to either a packed bed flow tube for detection of radioactively labeled nitrogen oxides (b), or to analytical devices for detection and characterization of also non-labeled molecules (c).

2.1 Production of ^{13}N

The production of ^{13}N isotopes *via* the reaction $^{16}\text{O}(p, \alpha)^{13}\text{N}$ has been described in detail before [12]. In brief, a flow of 10% O_2 (99.9995%, AirLiquid) in He (99.9999%, Messer) passed through a gas target at 1 L min^{-1} flow velocity and at 2 bar pressure that was continuously irradiated with an 11 MeV proton beam – provided by the accelerator facilities at Paul Scherrer Institute, Switzerland. The primary ^{13}N molecules and radicals were reduced to NO over a molybdenum catalyst at 653 K, immediately after the target cell. The resulting gas was continuously transported to the laboratory through a 580 m long capillary. The radiation chemistry in the target cell also led to the production of non-labeled nitrogen oxides at around $2 \times 10^{11} \text{ molecules cm}^{-3}$ from nitrogen impurities in the carrier gas supplies.

2.2 Synthesis of HNO_4

^{13}N labeled and/or non-labeled HNO_4 was continuously synthesised in the gas phase by reaction of NO_2 with HO_2 . For this, a $\text{H}_2\text{O}/\text{O}_2/\text{CO}/\text{NO}_2$ mixture in a N_2 (Carbagas, 99.999%) gas flow passing an 8 mm i.d. quartz tube was irradiated by an excimer UV lamp (Heraeus) emitting light at a wavelength of 172 nm. Typical mixing ratios of the gas phase species at atmospheric pressure were $3.5 \times 10^{18} \text{ molecules cm}^{-3}$ H_2O , $2.3 \times 10^{16} \text{ molecules cm}^{-3}$ CO , $1.3 \times 10^{16} \text{ molecules cm}^{-3}$ O_2 , and $9.4 \times 10^{12} \text{ molecules cm}^{-3}$ NO_2 . Ultrapure water (0.054 μS , Millipore) was dosed by passing the gas flow through a home-built, temperature regulated humidifier consisting of a heated Teflon tube immersed in water. The gases were mixed from certified gas bottles of synthetic air (Carbagas, 20% O_2 in N_2

(99.999%)), of CO (Carbagas, 10% CO in N_2 (99.999%)), and of NO (Carbagas, 10 ppm NO in N_2 (99.999%)) as source for NO_2 , see below.

NO_2 was quantitatively synthesized by mixing a gas flow containing NO , from the PROTRAC target and/or from the certified gas bottle, and O_3 in a reactor of 2 L volume. O_3 was produced by irradiation of a flow of dry synthetic air with a Hg pen-ray lamp at 185 nm. The irradiation time and the flow of O_2 were adjusted to achieve a small excess of O_3 for full conversion of NO to NO_2 , but not more than $2 \times 10^{12} \text{ molecules cm}^{-3}$ excess to prevent further oxidation of the NO_2 .

2.3 Detection of HNO_4 and by-products

A chemical ionization mass spectrometer was used to monitor HNO_4 in the gas phase. The mass spectrometer has been described elsewhere [15], the detection scheme was adapted from Slusher [10]. The strength of this mass spectrometer method is that – without further use of specific chemical traps – several nitrogen oxides can be detected simultaneously based on specific cluster ions [16]. These clusters were produced by reaction with SF_6^- in a home-made ionization chamber situated in front of the mass spectrometer entrance orifice. In detail, a flow of 600 mL min^{-1} of the gas flow exiting the HNO_4 synthesis was mixed with a flow of 1205 mL min^{-1} N_2 and SF_6^- at 11 mbar total pressure. The SF_6^- ions were produced by passing SF_6 (Carbagas, 1% SF_6 in Ar (99.999%)) in N_2 through a ^{210}Po -ionizer (NRD, p-2031). To enhance the formation of ions, a negative voltage of -136 V was applied to the ionizer and the inner walls of the ionisation chamber. Charged clusters entered the mass spectrometer from the ionization chamber *via* an orifice at -10 V .

The following clusters have been described and were also observed in this work: $(\text{HF})^- \text{NO}_4$ with mass 98 from reaction of HNO_4 with SF_6^- [10], $(\text{HF})^- \text{NO}_3$ with mass 82 from HNO_3 [16], $(\text{HF})^- \text{NO}_2$ with mass 66 for HNO_2 [17], NO_2^- with mass 46 for NO_2 [16]. A complication of mass spectrometry is that several different species might produce identical fragments. HNO_4 , for example, has been described to break apart upon reaction with SF_6^- leading also to the formation of $(\text{HF})^- \text{NO}_2$ clusters that are typically used to monitor HNO_2 [10]. To quantify this effect the gas flow containing the nitrogen oxides was heated to 373 K for quantitative destruction of HNO_4 to form NO_2 . HNO_4 is thermally unstable [18] and the exposure to 373 K at our experimental flow conditions led to a quantitative decomposition of HNO_4 as verified by observation of the mass spectrometer's signal at a mass to charge ratio (m/z) of 98. To heat the gas flow 2 m of the PFA tube were wrapped around an aluminium support and covered by temperature-regulated heating wire (Wisag AG, Switzerland). It was found that the $(\text{HF})^- \text{NO}_2$ signal decreased by about 10%. From this we conclude that the $(\text{HF})^- \text{NO}_2$ fragment at $m/z = 66$ has also a non-negligible contribution from HNO_4 at our detection conditions. We further found that $m/z = 66$ also rose in absence of nitrogen oxides, as soon as O_3 was added. This correlation of O_3 and the signal at $m/z = 66$ was observed earlier [19], and is assigned to $\text{O}_3^- (\text{H}_2\text{O})$ clusters of mass 66. To correct for this, and derive the fraction of the signal that is not

caused by O_3 , O_3 was also monitored at mass 48 (O_3^-). The ratio of $m/z = 48$ to $m/z = 66$ was determined in the absence of nitrogen oxides and used to compute the intensity of $m/z = 66$ due to O_3 during the synthesis. This later signal was then subtracted from the raw signal at $m/z = 66$ to give an estimate of the $m/z = 66$ traces originating from HNO_2 . No interferences were observed for $m/z = 82$ or $m/z = 46$. Overall, with this measurement method, HNO_4 , HNO_3 , and NO_2 can be monitored with high selectivity, while HNO_2 measurements are less reliable. The mass spectrometer data allow direct analysis of relative trends in the individual nitrogen oxide's abundance with changing synthesis settings. For a quantitative analysis the mass spectrometer needs to be calibrated.

Quantification of the nitrogen oxides in the reactor and calibration of the mass spectrometer was done by means of a chemiluminescence NO monitor equipped with a molybdenum converter (Monitor Labs 9841). This converter reduces nitrogen oxides to NO and its use thus allows detecting the sum of all nitrogen oxides present in a sample (NO_x), by-passing it selectively quantifies NO. Please note that the presence of CO interferes with the NO measurements, so that NO cannot be quantified in this study. NO_x measurements *via* the converter were not affected by the presence of CO, presumably because the molybdenum converter eliminates CO. To further differentiate individual nitrogen oxides selective chemical traps were used. The performance of the traps was verified by observing the individual traces in the mass spectrometer. HNO_3 is not detected by this NO monitor, because it is removed from the gas flow prior to entering the molybdenum converter by steel components of the instrument. Its concentration can be given by drop in the instrument's signal intensity when the synthesis is started. Scrubbing HNO_4 and HNO_2 from the gas phase in a carbonate trap and measuring the remaining nitrogen oxide content in the gas phase quantifies NO_2 . The carbonate trap was made from firebrick granulate that was soaked with 1.5% aqueous Na_2CO_3 (Fluka, p.a.) solution, dried, and placed in a 100×6 mm glass tube. The ends of the glass tube were filled with glass wool to keep the covered firebrick in its position. Due to their acidity, carbonate traps HNO_4 , and HNO_2 ; but neither NO_2 nor NO. HNO_4 was quantified by heating the gas flow to 373 K, by which HNO_4 is converted to NO_2 , before it enters the carbonate trap. The measured gas-phase concentration corresponds then to HNO_4 and NO_2 . From this measurement, also HNO_2 can be derived as fraction of nitrogen oxides that is removed by the carbonate trap. All this requires careful calibration of the nitrogen oxide analyzer that was done with a certified bottle of NO (Carbagas, 10 ppm NO in N_2 (99.999%)).

2.4 Packed bed flow tube

The main feature of the packed bed flow tube is a negative temperature gradient along a bed of packed ice spheres – 500 μm in diameter each – as described previously [14]. One end, where the gas flow enters the packed bed flow tube was cooled with a circulating cooling liquid regulated at 250 K. The other end where the gas flow exits the apparatus, was immersed in liquid nitrogen. The temperature inside the flow

tube was measured with a Pt-100 thermo element (MTS, Switzerland) prior to the measurements.

To start an experiment, a packed bed flow tube was placed in the apparatus and exposed to the temperature gradient for 30 min to allow the temperature equilibrium to be reached at any place in the ice flow tube. Then, the carrier gas containing the ^{13}N - and ^{14}N -nitrogen oxides was fed into the packed bed flow tube. After 30 min the experiment was stopped, and the flow tube was removed, sealed and immersed in an open bath of liquid nitrogen to stop any further migration of species. In some experiments, the gas flow passed a cooling trap prior to entering the packed bed flow tube to freeze out components from the carrier gas flow with a high partitioning tendency to surfaces. Different geometries and thus surface to volume ratios were used depending on the demands on the capacity. Typically, a quartz tube, 50 mm i.d. and 200 mm in length was filled with quartz spheres, to enhance the surface area, and cooled to 268 K by ethanol cooling liquid circulating around its wall. The cooling trap was operated at least 1 h prior to experiments.

The distribution of the ^{13}N -nitrogen oxides on the ice surface along the flow tube is the primary observable of the experiment and was measured by means of a coincident γ -counter. The coincident γ -counter consisted of two bismuth-germanate-detectors; 3 cm in diameter, mounted face to face with a gap of 35 mm. Lead shields were used to reduce the detection width to a slit of 5 mm distance. Coincident γ -counting leads to optimum counting efficiency and low background counting rates (1 cps or less), because annihilation of positrons following the β^+ -decay of ^{13}N results in two γ -rays in opposite direction to each other.

For each experiment, a new packed bed flow tube was prepared as described earlier [7, 14]: Spraying of ultra pure water into liquid nitrogen rapidly froze small ice droplets. After a minimum of 2 d of annealing at 253 K, the ice spheres were sieved with calibrated sieves (Retsch, Germany) to grain sizes between 400 and 600 μm , filled into a PFA tube (8 mm inner diameter, 360 mm length), and stored again for at least 12 h at -20°C . This preparation was done in a walk-in cold room, during transport to the laboratory, the ice columns were cooled with cooling elements in an insulated box. Based on the mass of the ice filling and the mean diameter of the spheres a mean ice surface area of the packed bed of 20 cm per cm length and a packing density of 70% can be calculated.

3. Results and discussion

Irradiation at 172 nm of a $\text{H}_2\text{O}/\text{NO}_2/\text{O}_2$ mixture leads to the production of OH and HO_2 radicals by photolysis of water (Eqs. 1 and 2), both of which react with NO_2 to form HNO_3 (Eq. 3) and HNO_4 (Eq. 4), respectively. Central to the synthesis of HNO_4 with high yields is to shift the OH to HO_2 ratio towards an excess of HO_2 and thus amplify HNO_4 yields. Fig. 2 shows that this can be achieved in the presence of CO as scavenger. CO reacts fast with OH but not with HO_2 (Eqs. 2 and 5) [20].



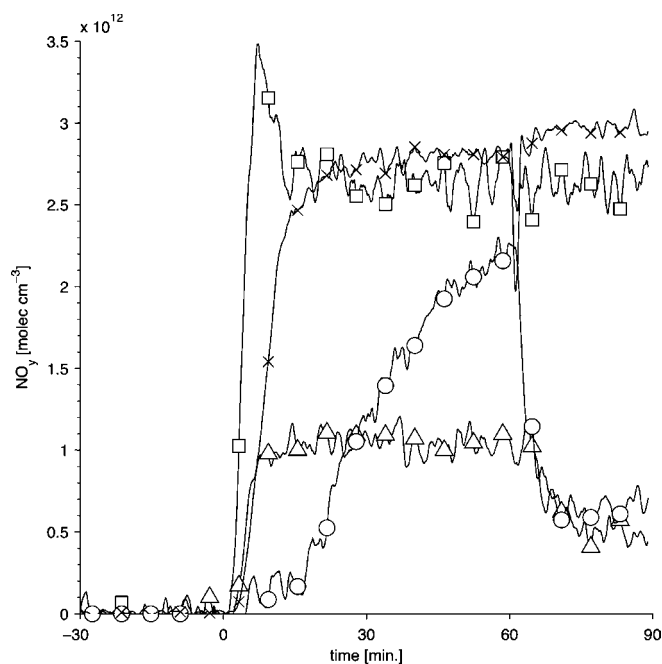


Fig. 2. Products of the HNO_4 synthesis with time at 8.7×10^{12} molecules cm^{-3} initial NO_2 . The line plot shows the calibrated traces as measured with the mass spectrometer of HNO_4 (line with crosses), HNO_3 (circles), HNO_2 (triangles), and NO_2 (squares). On the relative time axis 0 denotes the time when the NO_2 flow was switched on to start the synthesis of HNO_4 . 60 min later the gas flow was passed over a cooling trap at 268 K situated just after the reactor.



Fig. 2 displays the gas phase concentrations of HNO_4 , HNO_3 , HNO_2 , and NO_2 in the reactor with time as measured with the mass spectrometer during irradiation in absence (Fig. 2, -30 to 0 min) and in the presence of NO_2 (Fig. 2, 0 – 90 min). It can be clearly seen that, at a high concentration of 2×10^{16} molecules cm^{-3} CO, HNO_4 is the main product with a concentration in the reactor of 3×10^{12} molecules cm^{-3} . HNO_3 and HNO_2 are also detected but at lower concentrations of 2×10^{12} molecules cm^{-3} and 1×10^{12} molecules cm^{-3} , respectively. HNO_3 is most likely formed *via* Eq. (3). HNO_2 can potentially be formed by reaction of NO with OH, where NO comes from reaction of NO_2 with O- or with H-radicals. H-radicals are an intermediate product of the reaction 1 and 5, O-radicals originate from photolysis of O_3 .

Also shown is a significant decrease of 76% HNO_3 in gas-phase reaching the mass spectrometer when the flow is feed through a cooling trap at 268 K (Fig. 2, 60 – 90 min). This loss can be explained by the high tendency of HNO_3 to stick to surfaces even at high temperatures. The mass spectrometer traces of HNO_4 and of HNO_2 did also show a response to the cooling trap. But these are caused by variations in humidity in the chemical ionization mass spectrometer by adsorption of water in the cooling trap and not by changes in the concentration of HNO_4 or HNO_2 , respectively. This conclusion is supported by independent measurements of the total nitrogen oxide concentration in the gas

flow with the chemiluminescence detector the performance of which is unaffected by gas-phase humidity. The signal from this nitrogen oxide analyzer that is sensitive to NO, NO_2 , HNO_2 , and HNO_4 , but not to HNO_3 , did not show any reduction when the gas passed the cooling trap. Additionally, it is well known that the concentration of water in the chemical ionization chamber can significantly affect the formation and yield of ion production [16]. For example, water might exchange with HF in $(\text{HF})^-\text{NO}_4$ clusters of $m/z = 98$ leading to $(\text{H}_2\text{O})^-\text{NO}_4$ clusters of $m/z = 96$. A slight decrease in relative humidity, when the gas flow is fed over the cooling trap, might thus explain the higher abundance of $m/z = 98$ and the decrease in observed intensity of the $m/z = 96$ cluster (data not shown). Similarly, the cluster $(\text{HF})^-\text{NO}_2$ with $m/z = 66$ might be sensitive to humidity. Additionally, and likely more important, to derive the concentration of HNO_2 based on the measured trace with $m/z = 66$, the portion of the mass spectrometer signal originating from the $\text{O}_3^-\text{H}_2\text{O}$ cluster (also at $m/z = 66$) was subtracted (see Experimental). As the later cluster heavily depends on the water content, this analysis becomes questionable when humidity is not stable during an experiment. As the intensity of the cluster $(\text{H}_2\text{O})^-\text{NO}_3$ did not change during passage through the cooling trap, we conclude that the cluster $(\text{HF})^-\text{NO}_3$ does not respond to changes in humidity under our experimental conditions and consequently, the drop in signal intensity observed at $m/z = 82$ can be fully attributed to loss of HNO_3 from the gas phase. Note that the temperature of the cooling trap was always above the dew point of water in the carrier gas to prevent riming.

In summary, in presence of CO in large excess, HNO_4 , HNO_3 , HNO_2 , and NO_2 have been identified as products by mass spectrometer measurements. Calibration of the mass spectrometer traces by and comparison to measurements with a chemiluminescence analyzer showed that HNO_4 is the main product, but that substantial amounts of HNO_3 and HNO_2 are present. HNO_3 can be significantly reduced by use of a cooling trap at 268 K, whereas HNO_4 and HNO_2 pass this trap unhindered.

More information on the effect of CO on the product distribution of the photolysis can be seen in Fig. 3 showing the concentration of nitrogen oxides with increasing CO content in the gas phase. In the absence of CO, about 80% of the initial NO_2 is oxidized, forming primarily HNO_3 . This synthesis route to HNO_3 is well established and HNO_3 yields of up to 90% can be reached at higher humidity [12]. This approach has been used as HNO_3 source in a number of earlier experiments [21, 22]. The level of HNO_3 drops rapidly to below 20% with increasing concentration of CO in the reactor and, simultaneously, the HNO_4 share increases from below 5 to over 30%. The major leap in the HNO_4 yield is observed at CO concentrations of 1.0×10^{16} molecules cm^{-3} , further increase in CO seems to lead to no significant increases in HNO_4 yields, presumably because the self-reaction of HO_2 to form H_2O_2 becomes more important. H_2O_2 has not been quantified in this study due to a lack of a method to calibrate the mass spectrometer signal. A high count rate of $m/z = 140$ was observed and can be attributed to H_2O_2 at our experimental conditions. Bardwell *et al.* have observed and explained this mass as product of a multi-step reaction

from HO_2 and SF_6^- previously [23]. We have excluded the presence of HO_2 in the sample gas immediately before the sample inlet by adding NO_2 to the gas flow after the reactor. In the presence of HO_2 , HNO_4 should have been formed, which was not observed. We thus argue that the fragment of $m/z = 140$ also originates from H_2O_2 . HNO_2 shows no response to varying CO concentrations with a constant yield of about 10%. NO_2 concentration increases slightly from about 20–40% with increasing CO.

The observed trends for HNO_4 and HNO_3 with increasing CO as determined with the specific traps and the nitrogen oxide analyzer (Fig. 3) are supported by the mass spectrometer measurements. The very selective, but relative, raw mass spectrometer signals of both species at various CO concentrations show the same trend. In contrast, the mass spectrometer data of NO_2 indicate the highest yields in the absence of CO followed by a plateau with increasing CO levels, which is quite different from the increasing NO_2 levels with rising CO concentration as measured with the nitrogen oxide analyzer. An explanation might be that NO turns up as further by-product at high CO concentrations. NO does not interfere with the NO_2 signal of the mass spectrometer, but contributes to the NO_2 budget as determined with the carbonate trap and chemiluminescence analyzer. The same might hold for some organic nitrates that can potentially also be formed in the reactor during the photolysis in the presence of CO.

To increase readability, Figs. 2 and 3 do not show any error bars. Uncertainties of the mass spectrometer measurements, based on the standard deviation of 3 repeated experiments at $2.3 \times 10^{16} \text{ molecules cm}^{-3}$ CO, are 42% of the mean signal, 18, 14, and 4% for NO_2 , HNO_2 , HNO_3 , and HNO_4 . NO_2 is generally difficult to measure by chemical ionization mass spectrometry, because its reaction with SF_6^- is slow which makes this measurement method for NO_2 insensitive and uncertain [24]. The reproducibility of HNO_2 measurements is quite low, because of the intense data handling necessary to correct the raw signals for interferences. Measurements of HNO_3 by the chemical ionisation mass spectrometer are very sensitive and accurate, but HNO_3 might be lost at tubing walls during transport to the mass spectrometer resulting in a lower reproducibility of the amount that actually enters the mass spectrometer. HNO_4 measurements show an excellent reproducibility.

The main uncertainty of the chemiluminescence measurements originates most likely from fluctuations of the chemical trap performance. Standard deviations of 16, 19, 6, and 22% for NO_2 , HNO_2 , HNO_3 , and HNO_4 were determined.

To summarize, addition of CO to the gas phase leads to a significant increase of HNO_4 as product with a maximum yield of about 30% of the initial NO_2 . The fraction of HNO_3 decreases significantly with higher CO levels, from the main product in the absence of CO to a share smaller than the HNO_4 content at CO levels higher than $1.0 \times 10^{16} \text{ molecules cm}^{-3}$. HNO_2 , on the other hand, shows a rather invariant yield with higher CO levels and accounts for about 1/3 of the HNO_4 concentration. The use of a cold-trap at 268 K further reduces the HNO_3 mixing ratio in the gas flow.

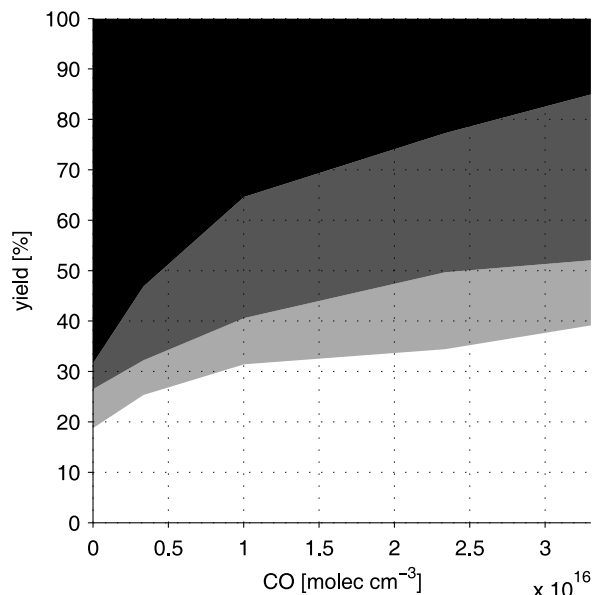


Fig. 3. Products of the HNO_4 synthesis with increasing CO concentration. The area graph displays the proportion of each nitrogen oxide as quantified by chemical traps and by the chemiluminescence detector relative to the amount of total nitrogen oxides: NO_2 (white), HNO_2 (light gray), HNO_4 (dark gray), HNO_3 (black).

4. Chromatography of ^{13}N -nitrogen oxides

Based on the above, the following settings were chosen for the production of ^{13}N labeled HNO_4 during the packed bed flow tube experiments: $2.3 \times 10^{16} \text{ molecules cm}^{-3}$ CO, $1.3 \times 10^{16} \text{ molecules cm}^{-3}$ O_2 , $9.4 \times 10^{12} \text{ molecules cm}^{-3}$ NO_2 , $3.5 \times 10^{18} \text{ molecules cm}^{-3}$ H_2O . With these settings about $2.6 \times 10^{12} \text{ molecules cm}^{-3}$ HNO_4 , $2.2 \times 10^{12} \text{ molecules cm}^{-3}$ HNO_3 , $1.4 \times 10^{12} \text{ molecules cm}^{-3}$ HNO_2 , and $3.2 \times 10^{12} \text{ molecules cm}^{-3}$ NO_2 exited the reactor.

The resulting distribution of this mixture along the packed bed flow tube, as shown in Fig. 4a, reveals three distinct zones of increased radioactive decays centred around temperatures of 267 K with a 95% confidence interval of 252–282 K, 184 K (170–198 K), and of 126 K (116–136 K). The confidence interval reflects uncertainties in determining the centre position of the zone by a Gaussian fit to the data and uncertainties in temperature determination at that position by linear regressions.

The evolution of these peaks is a direct consequence of the partitioning of each species between the gas phase passing through the flow tube and the surface of the packed bed [13]. As this interaction is both strongly temperature dependent and species-specific, mixtures of trace gases are separated during their migration along the packed bed process reflecting their individual partitioning behaviour [14]. Thus the results presented in Fig. 4 indicate that the gas flow contains 3 types of nitrogen oxides species, with weak, intermediate and strong partitioning to the ice phase, respectively.

When the gas flow is passed *via* a cooling trap at 268 K prior to entering the packed bed flow tube, the radioactive decays at the beginning of the packed bed do not exceed the background level and only two peaks are evident at 189 K (175–204 K) and at 135 K (126–144 K). The first peak appears at an identical position and temperature as the cor-

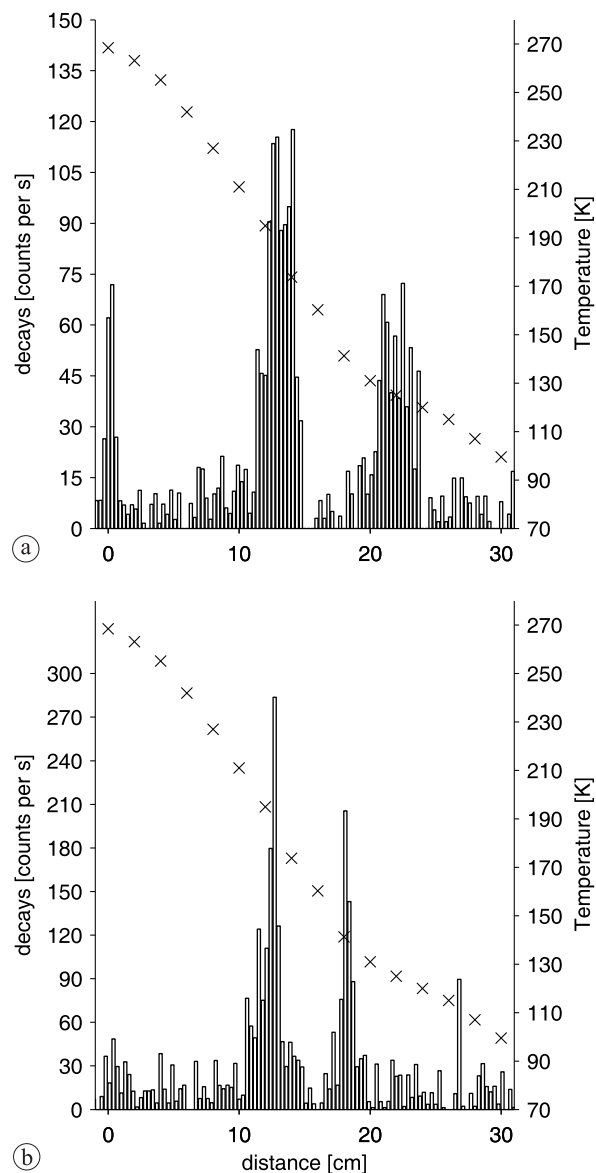


Fig. 4. The distribution of radioactive decays from ^{13}N -labeled nitrogen oxides along packed bed flow tubes. Zero denotes the beginning of the ice bed. Also shown are the temperature profiles inside the flow tube (crosses). (a) The gas flow from the synthesis was directly passed over the packed bed flow tube for 30 min. (b) The gas flow passed a cooling trap at 268 K prior to the packed bed flow tube.

responding peak in Fig. 4a. The second peak is shifted to a shorter distance and slightly higher temperature, but as the confidence intervals overlap this difference is statistically not significant.

The vanished peak at 267 K can clearly be assigned to HNO_3 based on measurements with the mass spectrometer that showed that HNO_3 is the only species scrubbed by this cold trap. The strong interaction with ice, or dominant partitioning to the surface at relatively high temperatures, is also supported by recent IUPAC recommendations on the partitioning of HNO_3 between ice and air, which predict a high surface concentration of 2×10^3 molecules cm^{-2} in equilibrium for each gas-phase molecule cm^{-3} at 267 K [25]. The partitioning of NO_2 and HNO_2 to ice is much weaker compared to HNO_3 : Significant adsorption of NO_2 to ice has not been observed at temperatures above 195 K [26, 27]. HNO_2 partitioning to ice surfaces occurs at higher tem-

perature (above 170 K) [7, 28, 29]. Consequently, we can assign HNO_2 deposition to the second zone at 184 K and NO_2 to the third zone at 126 K. Again, the current IUPAC recommendations for HNO_2 support this conclusion with 1×10^4 molecules cm^{-2} HNO_2 on the surface per molecule cm^{-3} in the gas-phase at 184 K.

This assessment of HNO_3 , HNO_2 , and NO_2 is supported by our earlier experiments where we have used selective traps to identify the deposition zones of nitrogen oxides along a negative temperature gradient in a packed bed flow tube [14]. During those earlier experiments settings such as flow velocity (75 and $360 \text{ cm}^3 \text{ min}^{-1}$) and ice surface area in the packed bed flow tube (4 and $10.9 \text{ cm}^2 \text{ cm}^{-1}$) were similar but not identical to those in our current investigation. However, systematic variation of these settings during our earlier work was found not to result in modified retention behaviour. Direct comparison of the deposition properties seems thus well suited. NO_2 was found to migrate to a position with a temperature of 132 K with a 95% confidence interval of 18 single experiments of ± 14 K, which is in excellent agreement with 5 recent experiments, for which a mean of 130 K (± 9 K) can be determined. HNO_2 was found to migrate to temperatures at 186 K (± 20 K for 8 experiments), which overlaps with the intermediate peak as presented in Fig. Fig. 4 at 191 K (± 17 K for 5 experiments).

Li *et al.* have observed that HNO_4 is released from ice surfaces at temperatures above 210 K, whereas HNO_3 was only released at higher temperatures of 246 K or above [30]. These results imply for our experimental set-up that HNO_4 deposits at lower temperatures than HNO_3 , *i.e.* at the same position as HNO_2 in the second peak (Fig. 4a). This conclusion is supported by comparing the peak areas as measure for the amount of nitrogen oxides deposited to the concentration of nitrogen oxides in the carrier gas as determined by chemiluminescence measurements. For this, the Gauss fits to the distribution of radioactive decays along the packed bed flow tube were integrated. The areas of peak 1 : peak 2 : peak 3 scale with the ratio 0.5 : 1.7 : 1. Taking that pure NO_2 deposits in peak 3 and pure HNO_3 in peak 1 we can compare this to the ratio of NO_2 : HNO_3 of 0.7 as determined by quantification of the nitrogen oxide budget by the chemiluminescence analyzer (Fig. 3). This agreement is excellent, taking into account that a fraction of HNO_3 is lost during its way to the packed bed flow tube by surface adsorption on the tubing walls. The mass balance analysis of nitrogen oxides further reveals that neither HNO_2 , nor HNO_4 alone, can explain the observed high intensity of peak 2. The ratio of HNO_2 to NO_2 is only 0.4 and the ratio of HNO_4 to NO_2 is 0.8; both ratios are less than the ratio of the area of peak 2 to peak 3 of 1.7. Thus it is most likely that both species together deposit in peak 2.

The uptake to ice surfaces heavily depends on the amount of total uptake to the surface, as at high surface concentrations, adsorbate–adsorbate interactions evolve. For our experiments, a surface concentration of HNO_4 on the ice of 1×10^{14} – 4×10^{14} molecules cm^{-2} can be calculated. For this calculation, a typical length of the deposition zone of 5 cm, HNO_4 gas phase concentration entering the packed bed flow tube of 1×10^{12} – 5×10^{12} molecules cm^{-3} with a flow of 300 mL min^{-1} for 30 min, were used. The resulting surface concentration is significantly lower than during the early

study by Li *et al.* in which a formal monolayer, here defined as 1×10^{15} molecules cm⁻², was exceeded [30].

We conclude that the interaction of HNO₄ with ice surfaces is significantly weaker than observed for HNO₃, it rather resembles the interaction of HNO₂ with ice. One might thus expect that the partitioning coefficient at the temperature of peak 2 for HNO₄ is similar to the recommendations for HNO₂, and we propose the same partitioning coefficient K_{LinC} of 7.6×10^{-5} cm⁻¹ also for HNO₄ at 189 K. The partitioning coefficient K_{LinC} is defined as concentration of adsorbed species per surface area divided by concentration of gas-phase species per volume in equilibrium and is frequently used for parameterization of surface uptake in atmospheric chemistry models.

5. Conclusion and outlook

A new synthesis route to H¹³NO₄ was developed based on the gas-phase reaction of ¹³NO₂ + HO₂. At high concentrations of CO, HNO₄ is the main product with a yield of 30%. HNO₃ and HNO₂ are the most important nitrogen oxide by-products. HNO₃ can be scrubbed from the gas flow in a cold trap at 268 K. Exposure of this mixture to a temperature gradient along a packed ice bed leads to separation of HNO₃ from HNO₂, HNO₄, and from NO₂. This migration behaviour reveals that the interaction of HNO₄ with ice surfaces is similar to that of HNO₂-ice but much weaker than the HNO₃-ice interaction. Thus, the surface partitioning coefficient (K_{LinC}) that quantitatively describes the uptake to the ice surface lies in the order of 7.6×10^{-5} cm⁻¹ also for HNO₄ at 189 K. This implies that the uptake of HNO₄ by surface snow in Antarctica or ice crystals in the upper troposphere, where temperatures of 190 K can be reached, is a very potential loss process.

Precise measurement of the surface partitioning and especially its temperature dependence is urgently recommended. For this isothermal chromatographic methods are well suited [7, 29]. The advantage of isothermal methods is that the highly temperature-dependent partitioning coefficient is the observable of such experiments, and can be directly measured at the temperatures of interest. The strength of the gradient method is rather that it directly reflects the relative intensity of trace-gas-ice interactions for mixtures exposed to the ice surface.

Scrubbing of HNO₂ and HNO₃ from the gas flow is required as the concentration of HNO₂ in the synthesis presented here is too high for isothermal experiments.

Acknowledgment. We gratefully thank M. Birrer for the excellent technical support. We acknowledge the staff of the PSI accelerator facilities for supplying stable proton beams. We thank I. Zimmermann and J. Graell for their work on this project during their internships with us. We thank R. Eichler for discussion on the thermochromatography experiments. This project was supported by the Swiss National Science Foundation, project no. 200021_121857 and the EU FP6 SCOUT-O3 project (GOCE-CT-2004- 505390) funded through the Swiss Federal Office of Education and Science.

References

1. Huthwelker, T., Ammann, M., Peter, T.: The uptake of acidic gases on ice. Chem. Rev. **106**, 1375–1444 (2006).

2. Abbatt, J.: Interactions of atmospheric trace gases with ice surfaces: Adsorption and reaction. Chem. Rev. **103**, 4783–4800 (2003).
3. Popp, P. J., Marcy, T. P., Watts, L. A., Gao, R. S., Fahey, D. W., Weinstock, E. M., Smith, J. B., Herman, R. L., Troy, R. F., Webster, C. R., Christensen, L. E., Baumgardner, D. G., Voigt, C., Kaercher, B., Wilson, J. C., Mahoney, M. J., Jensen, E. J., Bui, T. P.: Condensed-phase nitric acid in a tropical subvisible cirrus cloud. Geophys. Res. Lett. **34**, L24812 (2007).
4. Grannas, A. M., Jones, A. E., Dibb, J., Ammann, M., Anastasio, C., Beine, H., Bergin, M., Bottenheim, J., Boxe, C. S., Carver, G., Chen, G., Crawford, J. H., Dominé, F., Frey, M. M., Guzman, M. I., Heard, D. E., Helmig, D., Hoffmann, M. R., Honrath, R., Huey, L. G., Hutterli, M., Jacob, H.-W., Klán, P., Lefer, B., McConnell, J., Plane, J., Sander, R., Savarino, J., Shepson, P. B., Simpson, W. R., Sodeau, J. R., Von Glasow, R., Weller, R., Wolff, E. W., Zhu, T.: An overview of snow photochemistry: Evidence, mechanisms and impacts. Atmos. Chem. Phys. **7**, 4329–4373 (2007).
5. Dominé, F., Shepson, P.: Air-snow interactions and atmospheric chemistry. Science **297**, 1506–1510 (2002).
6. Pinzer, B., Kerbrat, M., Huthwelker, T., Gäggeler, H. W., Schneebeli, M., Ammann, M.: Diffusion of NO_x and HONO in snow: A laboratory study. J. Geophys. Res. **115**, D03304 (2010).
7. Kerbrat, M., Huthwelker, T., Gäggeler, H. W., Ammann, M.: Interaction of nitrous acid with polycrystalline ice: Adsorption on the surface and diffusion into the bulk. J. Phys. Chem. C **114**, 2208–2219 (2010).
8. Slusher, D., Huey, L., Tanner, D., Chen, G., Davis, D., Buhr, M., Nowak, J., Eisele, F., Kosciuch, E., Mauldin, R., Lefer, B., Shetter, R., Dibb, J.: Measurements of pernitric acid at the South Pole during ISCAT 2000. Geophys. Res. Lett. **29** (2002).
9. Jaeglé, L., Jacob, D., Brune, W., Wennberg, P.: Chemistry of HO₂ radicals in the upper troposphere. Atmos. Environ. **35**, 469–489 (2001).
10. Slusher, D., Pitteri, S., Haman, B., Tanner, D., Huey, L.: A chemical ionization technique for measurement of pernitric acid in the upper troposphere and the polar boundary layer. Geophys. Res. Lett. **28**, 3875–3878 (2001).
11. Staikova, M., Donaldson, A., Francisco, J.: Overtone-induced reactions on the HO₂/NO₂ potential surface. J. Phys. Chem. A **106**, 3023–3028 (2002).
12. Ammann, M.: Using ¹³N as tracer in heterogeneous atmospheric chemistry experiments. Radiochim. Acta **89**, 831–838 (2001).
13. Eichler, B., Zvara, I.: Evaluation of the enthalpy of adsorption from thermochromatographical data. Radiochim. Acta **30**, 233–238 (1982).
14. Bartels-Rausch, T., Eichler, B., Zimmermann, P., Gäggeler, H. W., Ammann, M.: The adsorption enthalpy of nitrogen oxides on crystalline ice. Atmos. Chem. Phys. **2**, 235–247 (2002).
15. Guimbaud, C., Bartels-Rausch, T., Ammann, M.: An atmospheric pressure chemical ionization mass spectrometer (APCI-MS) combined with a chromatographic technique to measure the adsorption enthalpy of acetone on ice. Int. J. Mass. Spectrom. **226**, 279–290 (2003).
16. Huey, L. G.: Measurement of trace atmospheric species by chemical ionization mass spectrometry: Speciation of reactive nitrogen and future directions. Mass. Spectrom. Rev. **26**, 166–184 (2007).
17. Longfellow, C., Imamura, T., Ravishankara, A., Hanson, D.: HONO solubility and heterogeneous reactivity on sulfuric acid surfaces. J. Phys. Chem. A **102**, 3323–3332 (1998).
18. Zabel, F.: Unimolecular decomposition of peroxyxynitrates. Z. Phys. Chem. **188**, 119–142 (1995).
19. Abbatt, J., Oldridge, N., Symington, A., Chukalovskiy, V., McWhinney, R. D., Sjostedt, S., Cox, R. A.: Release of gas-phase halogens by photolytic generation of OH in frozen halide-nitrate solutions: An active halogen formation mechanism? J. Phys. Chem. A **114**, 6527–6533 (2010).
20. Schultz, M., Heitlinger, M., Mihelcic, D., Volzthomas, A.: Calibration source for peroxy-radicals with built-in actinometry using H₂O and O₂ photolysis at 185 nm. J. Geophys. Res.-Atmos. **100**, 18811–18816 (1995).
21. Vlasenko, A., Huthwelker, T., Gäggeler, H. W., Ammann, M.: Kinetics of the heterogeneous reaction of nitric acid with mineral

- dust particles: An aerosol flowtube study. *Phys. Chem. Chem. Phys.* **11**, 7921–7930 (2009).
22. Guimbaud, C., Arens, F., Gutzwiller, L., Gäggeler, H. W., Ammann, M.: Uptake of HNO_3 to deliquescent sea-salt particles: A study using the short-lived radioactive isotope tracer N-13. *Atmos. Chem. Phys.* **2**, 249–257 (2002).
23. Bardwell, M., Bacak, A., Raventos, M., Percival, C., Sanchez-Reyna, G., Shallcross, D.: Kinetics of the $\text{HO}_2 + \text{NO}$ reaction: A temperature and pressure dependence study using chemical ionisation mass spectrometry. *Phys. Chem. Chem. Phys.* **5**, 2381–2385 (2003).
24. Huey, L., Hanson, D., Howard, C.: Reactions of SF_6^- and I^- with atmospheric trace gases. *J. Phys. Chem.* **99**, 5001–5008 (1995).
25. Ammann, M., Atkinson, R., Cox, R., Crowley, J., Hynes, R., Jenkin, M., Rossi, M., Troe, J., Wallington, T., IUPAC Subcommittee: Evaluated kinetic and photochemical data for atmospheric chemistry: Heterogeneous reactions on ice. <http://www.iupac-kinetic.ch.cam.ac.uk/index.html> (2008).
26. Saastad, O., Ellermann, T., Nielsen, C.: On the adsorption of NO and NO_2 on cold $\text{H}_2\text{O}/\text{H}_2\text{SO}_4$ surfaces. *Geophys. Res. Lett.* **20**, 1191–1193 (1993).
27. Leu, M.: Heterogeneous reactions of N_2O_5 with H_2O and HCl on ice surfaces – implications for antarctic ozone depletion. *Geophys. Res. Lett.* **15**, 851–854 (1988).
28. Fenter, F., Rossi, M.: Heterogeneous kinetics of HONO on H_2SO_4 solutions and on ice: Activation of HCl. *J. Phys. Chem.* **100**, 13765–13775 (1996).
29. Chu, L., Diao, G., Chu, L.: Heterogeneous interaction and reaction of HONO on ice films between 173 and 230 K. *J. Phys. Chem. A* **104**, 3150–3158 (2000).
30. Li, Z., Friedl, R., Moore, S., Sander, S.: Interaction of peroxyxynitric acid with solid H_2O ice. *J. Geophys. Res.* **101**, 6795–6802 (1996).